A New Parametric GLRT for Multichannel Adaptive Signal Detection

Pu Wang, *Student Member, IEEE*, Hongbin Li, *Senior Member, IEEE*, and Braham Himed, *Fellow, IEEE*

***Abstract*—A parametric generalized likelihood ratio test (GLRT) for multichannel signal detection in spatially and temporally colored disturbance was recently introduced by modeling the disturbance as a multichannel autoregressive (AR) process. The detector, however, involves a highly nonlinear maximum likelihood estimation procedure, which was solved via a two-dimensional iterative search method initialized by a suboptimal estimator. In this paper, we present a simplified GLRT along with a new estimator for the problem. Both the estimator and the GLRT are derived in closed form at considerably lower complexity. With adequate training data, the new GLRT achieves a similar detection performance as the original one. However, for the more interesting case of limited training, the original GLRT may become inferior due to poor initialization. Because of its simpler form, the new GLRT also offers additional insight into the parametric multichannel signal detection problem. The performance of the proposed detector is assessed using both a simulated dataset, which was generated using multichannel AR models, and the KASSPER dataset, a widely used dataset with challenging heterogeneous effects found in real-world environments.**

***Index Terms*—Generalized likelihood ratio test, maximum likelihood estimation, parametric detection, space-time adaptive signal processing.**

I. Introduction

We consider multichannel signal detection in the presence of spatially and temporally colored disturbance, a problem also known as space-time adaptive processing (STAP) in radars [1]. Although the optimal matched filter (MF) is well understood, which performs joint spatial and temporal whitening using the space-time covariance matrix of the disturbance, this matrix is rarely known *a priori* and has to be replaced by some estimate, e.g., the sample covariance matrix obtained from homogeneous and target-free training data. A number of sample covariance matrix-based STAP detectors have been proposed (e.g., [2]–[6]). While these classical detectors set a good understanding of the multichannel signal detection problem, the challenge with them is that training data are often limited in many practical scenarios, e.g., detection in heterogeneous, dense-target, and/or multistatic induced nonstationary environments, which causes significant performance loss due to lack of sufficient secondary data that are needed to form a reliable covariance matrix estimate. This has led to recent development of STAP techniques with reduced training requirement, including partially adaptive or reduced-rank detection (e.g., [7]–[11]), parametric STAP detection [12]–[22], and others.

Parametric STAP detectors have recently gained considerable interest due to their remarkable ability of offering significant performance improvement over classical detectors in training limited cases. Specifically, the parametric adaptive matched filter (PAMF) [12], one of the first in this class, models the disturbance signal as a parametric multichannel autoregressive (AR) process. The parametric model allows signal whitening through an inverse moving-average filter, which replaces the standard whitening process using a full-dimensional space-time covariance matrix estimate found in classical STAP detectors. The immediate benefit brought by the parametric model is reduced unknown parameters to be estimated and, in turn, reduced training and computational requirements. The multichannel AR process has been found to be an effective tool to model real-world airborne radar clutter for STAP detection [14], [23], [24]. It is also versatile in capturing the temporal and spatial correlation of disturbance signals in other radar and array processing applications (e.g., [13], [25], and [26]). The PAMF detector is shown to be equivalent to a parametric Rao detector in [16]. The equivalence leads to analytical expressions for the asymptotic performance of the PAMF detector. Efficient implementations of the PAMF detector capitalizing on the inherent computational structure of the multichannel AR model are reported in [17] and [18]. Meanwhile, extensions of the multichannel AR modeling to nonstationary cases for STAP detection are investigated in [19]–[22].

The parametric generalized likelihood ratio test (GLRT) [16] is a recent addition into the parametric STAP family. An interesting observation made in [16] is that it is possible to trade range training with the number of pulses within a coherent processing interval (CPI). Specifically, the traditional way of learning the clutter statistic is to use the signals received over adjacent range cells near the test range as the training signals, assuming that the target is a rare event and that the clutter statistic does not change much over the neighborhood of the cell under test. This assumption is clearly violated in heterogeneous dense-target environments, which is why the sample covariance matrix-based detectors do not perform well in such cases. In contrast, [16] shows that the clutter statistic can be extracted from the temporal pulses over a CPI; in the extreme case, this can be achieved exclusively from the test signal, without using any range training, provided that the

Manuscript received April 13, 2009; accepted July 31, 2009. First published August 21, 2009; current version published December 16, 2009. The associate editor coordinating the review of this manuscript and approving it for publication was Prof. Xiang-Gen Xia. This work was supported by the Air Force Research Laboratory under Contract FA8750-05-2-0001 and by the Air Force Office of Scientific Research under Grant FA9550-09-1-0310.

P. Wang and H. Li are with the Department of Electrical and Computer Engineering, Stevens Institute of Technology, Hoboken, NJ 07030 USA (e-mail: pwang4@stevens.edu; Hongbin.Li@stevens.edu).

B. Himed is with the Radar Signal Processing Technology Branch, Air Force Research Laboratory, Dayton, OH 45433 USA (e-mail: Braham.Himed@wpafb.af.mil).

Digital Object Identifier 10.1109/TSP.2009.2030835

number of pulses is large enough. The performance of the parametric GLRT has been examined using simulated and real data in various training limited cases [23], [24].

There are still critical unresolved issues with the parametric GLRT. Specifically, it involves highly nonlinear parameter estimation that has no closed-form solution. An iterative search-based procedure is employed in [16], which is seen to be computationally intensive. Moreover, the iterative searching requires an initial guess of the unknown parameter. A two-step estimator is presented for that purpose, which starts with a least squares (LS) estimation step by ignoring the temporal/spatial correlation, followed by a refining step. While this estimator is an asymptotic maximum likelihood (AML) estimator, its performance is limited by the coarse LS estimator and, as we show in Section V, may not perform well when the number of pulses is small. Finally, the parametric GLRT, due to its complicated nonlinear form, offers little insight into how it functions. This is different from other parametric STAP detectors (e.g., [14] and [15]), which have a clear interpretation of sequential temporal and spatial whitening (see discussions in Section IV for details).

To address the above issues, we present herein a new estimator for the estimation problem underlying the parametric GLRT. The new estimator is in closed form and computationally simple. Unlike the earlier AML estimator, it does not need an initial guess and, thus, is not hindered by poor initialization. The new estimator also leads to a simplified parametric GLRT, offering additional insight unavailable with the original GLRT. In general, the new GLRT achieves similar detection performance as the original one. But in the more challenging case when the number of pulses is limited, the new GLRT may outperform the original GLRT (which employs an iterative search-based estimation procedure initialized by the AML estimator). The performance loss of the latter is primarily due to the poor initial parameter estimate provided by the AML estimator.

The remainder of this paper is organized as follows. Section II contains the data model and a summary of the original GLRT of [16], where an underlying nonlinear amplitude estimation problem is also highlighted. A new amplitude estimator is introduced in Section III, which leads to a simplified parametric GLRT presented in Section IV. Numerical results and conclusions are provided in Sections V and VI, respectively.

II. Data Model and Parametric GLRT

A. Data Model

The problem of interest is to detect a $JN\times 1$ multichannel signal $\mathbf{s}$ with *unknown* amplitude α in the presence of spatially and temporally correlated disturbance (e.g., [1])

$$\begin{aligned} H_0:&\quad \mathbf{x}_0=\mathbf{d}_0\\ H_1:&\quad \mathbf{x}_0=\alpha\mathbf{s}+\mathbf{d}_0 \end{aligned} \tag{1}$$

where J denotes the number of spatial channels and N the number of temporal observations (i.e., snapshots). It will be convenient to express the $JN\times 1$ vectors in terms of their spatial $J\times 1$ components, i.e.,

$$\mathbf{s}=\left[\mathbf{s}^T(0),\quad \ldots,\quad \mathbf{s}^T(N-1)\right]^T \tag{2}$$

and similarly $\mathbf{d}_0$ and $\mathbf{x}_0$ are decomposed into $\mathbf{d}_0(n)$ and $\mathbf{x}_0(n)$, respectively. In the sequel, $\mathbf{x}_0(n)$ is referred to as the *test signal,* $\mathbf{s}(n)$ as the *steering vector* (assumed known to the detector), and $\mathbf{d}_0(n)$ as the *disturbance signal* (i.e., clutter and noise) that may be correlated in space and time. In addition to the test signal $\mathbf{x}_0(n)$, there may be a set of *training* or *secondary* signals $\mathbf{x}_k(n)$, $k=1,\ldots,K$, that are target-free: $\mathbf{x}_k(n)=\mathbf{d}_k(n)$.

The binary composite hypothesis testing problem is to select between $H_0:\alpha=0$ and $H_1:\alpha\neq 0$. A standard assumption in STAP detection (e.g., [1]–[8]) is that the disturbance signals $\{\mathbf{d}_k\}_{k=0}^K$ are independent and identically distributed (i.i.d.) with distribution $\mathcal{CN}(\mathbf{0},\mathbf{R})$, where $\mathbf{R}$ is the *unknown* space-time covariance matrix. The parametric STAP detectors [12], [14]–[16] further assume that the disturbance signal $\mathbf{d}_k(n), k=0,\ldots,K$, can be modeled as a J-channel $\mathrm{AR}(P)$ process

$$\mathbf{d}_k(n)=-\sum_{i=1}^{P}\mathbf{A}^H(i)\mathbf{d}_k(n-i)+\boldsymbol{\varepsilon}_k(n) \tag{3}$$

where $\{\mathbf{A}^H(i)\}_{i=1}^P$ denotes the *unknown* $J\times J$ AR coefficient matrices and $\boldsymbol{\varepsilon}_k(n)$ denotes the $J\times 1$ spatial noise vectors that are assumed to be temporally white but spatially colored Gaussian noise $\boldsymbol{\varepsilon}_k(n)\sim\mathcal{CN}(\mathbf{0},\mathbf{Q})$, where $\mathbf{Q}$ denotes the *unknown* $J\times J$ spatial covariance matrix.

B. Parametric GLRT

To introduce the necessary notation and also to facilitate comparison, we briefly summarize the parametric GLRT [16] as follows. The parametric GLRT first finds the ML estimates (MLEs) of the unknown parameters under both hypotheses, which are next used to compute the test statistics. Amplitude estimation under H_1 turns out to be the key problem, as the other parameters can be readily obtained once an estimate of α is available. Specifically, the MLE of α is given by

$$\hat{\alpha}_{\mathrm{ML}}=\arg\min_{\alpha}\left|\hat{\mathbf{R}}_{xx}(\alpha)-\hat{\mathbf{R}}_{yx}^H(\alpha)\hat{\mathbf{R}}_{yy}^{-1}(\alpha)\hat{\mathbf{R}}_{yx}(\alpha)\right| \tag{4}$$

where $\hat{\mathbf{R}}_{xx}(\alpha)$, $\hat{\mathbf{R}}_{yy}(\alpha)$, and $\hat{\mathbf{R}}_{yx}(\alpha)$ are $J\times J$, $JP\times JP$, and $JP\times J$ matrices defined as

$$\begin{aligned}\hat{\mathbf{R}}_{xx}(\alpha)=&\sum_{k=1}^{K}\sum_{n=P}^{N-1}\mathbf{x}_k(n)\mathbf{x}_k^H(n)\\&+\sum_{n=P}^{N-1}\left[\mathbf{x}_0(n)-\alpha\mathbf{s}(n)\right]\left[\mathbf{x}_0(n)-\alpha\mathbf{s}(n)\right]^H\end{aligned} \tag{5}$$

$$\begin{aligned}\hat{\mathbf{R}}_{yy}(\alpha)=&\sum_{k=1}^{K}\sum_{n=P}^{N-1}\mathbf{y}_k(n)\mathbf{y}_k^H(n)\\&+\sum_{n=P}^{N-1}\left[\mathbf{y}_0(n)-\alpha\mathbf{t}(n)\right]\left[\mathbf{y}_0(n)-\alpha\mathbf{t}(n)\right]^H\end{aligned} \tag{6}$$

$$\begin{aligned}\hat{\mathbf{R}}_{yx}(\alpha)=&\sum_{k=1}^{K}\sum_{n=P}^{N-1}\mathbf{y}_k(n)\mathbf{x}_k^H(n)\\&+\sum_{n=P}^{N-1}\left[\mathbf{y}_0(n)-\alpha\mathbf{t}(n)\right]\left[\mathbf{x}_0(n)-\alpha\mathbf{s}(n)\right]^H\end{aligned} \tag{7}$$

and the regression vectors are defined as $\mathbf{t}(n) = [\mathbf{s}^T(n-1),\ldots,\mathbf{s}^T(n-P)]^T \in \mathbb{C}^{JP\times 1}$ and $\mathbf{y}_k(n) = [\mathbf{x}_k^T(n-1),\ldots,\mathbf{x}_k^T(n-P)]^T \in \mathbb{C}^{JP\times 1}$, $k=0,\ldots,K$. Once $\hat{\alpha}_{\mathrm{ML}}$ is obtained, the parametric GLRT is given by

$$T_{\mathrm{GLRT}} = 2L\ln\frac{|\hat{\mathbf{Q}}_{\mathrm{ML},0}|}{|\hat{\mathbf{Q}}_{\mathrm{ML},1}|} \underset{H_0}{\overset{H_1}{\gtrless}} \gamma_{\mathrm{GLRT}} \tag{8}$$

where[1] $L=(K+1)(N-P)$, γ_{GLRT} denotes the corresponding test threshold and $\hat{\mathbf{Q}}_{\mathrm{ML},0}$ and $\hat{\mathbf{Q}}_{\mathrm{ML},1}$ denote the ML estimates of the spatial covariance matrix under the null and alternative hypotheses

$$\hat{\mathbf{Q}}_{\mathrm{ML},0} = \hat{\mathbf{Q}}(\alpha)|_{\alpha=0} \tag{9}$$

$$\hat{\mathbf{Q}}_{\mathrm{ML},1} = \hat{\mathbf{Q}}(\alpha)|_{\alpha=\hat{\alpha}_{\mathrm{ML}}} \tag{10}$$

with

$$\hat{\mathbf{Q}}(\alpha) = \frac{1}{L}\left(\hat{\mathbf{R}}_{xx}(\alpha) - \hat{\mathbf{R}}_{yx}^H(\alpha)\hat{\mathbf{R}}_{yy}^{-1}(\alpha)\hat{\mathbf{R}}_{yx}(\alpha)\right). \tag{11}$$

The MLE (4) is highly nonlinear and cannot be solved in closed form. Iterative search over a two-dimensional parameter space (note that α is complex-valued) is typically employed, which is computationally intensive (as the matrix determinant has to be evaluated for every update of α) and, in general, converges only to a local minimum. To address this problem, an AML estimator was introduced in [16]. The AML estimator involves a two-step process. In particular, it first computes the LS of the amplitude

$$\hat{\alpha}_{\mathrm{LS}} = \frac{\mathbf{s}^H\mathbf{x}_0}{\mathbf{s}^H\mathbf{s}} \tag{12}$$

which effectively ignores the spatiotemporal correlation of the disturbance signal. Then, the initial estimate is refined through a weighed LS process (see [16] for details). Although the AML estimate can be shown to be asymptotically efficient, it is affected by the limited performance of the initializing LS estimator, in particular when the data size is small.

In closing this section, we briefly comment on the stability issue. In general, the multichannel AR process used to model the disturbance signal has to be stable to ensure that the resulting AR signal is wide-sense stationary [27]. A constrained ML estimator that maximizes the likelihood function under the constraint that the AR coefficient matrices form a stable multichannel filter is highly involved and generally not suitable for practical applications. In contrast, the estimators considered in this paper, including the ML and AML estimators as well as the one introduced in the next section, do not impose this constraint in the interest of computational simplicity. Although the estimated AR model obtained by any of these estimators is not guaranteed to be stable, extensive numerical studies using simulated and experimental data show that these unconstrained estimators yield good estimation and detection performance at acceptable complexity.

[1]While the scaling factor L can be dropped from the test statistic, it was retained in [16] to simplify the asymptotic analysis.

III. Amplitude Estimation

The exact MLE (4) minimizes the determinant of the α-dependent matrix

$$\hat{\mathbf{R}}_{xx}(\alpha) - \hat{\mathbf{R}}_{yx}^H(\alpha)\hat{\mathbf{R}}_{yy}^{-1}(\alpha)\hat{\mathbf{R}}_{yx}(\alpha)$$

which is the Schur complement (see, e.g., [28]) of the block matrix $\hat{\mathbf{R}}(\alpha)$

$$\hat{\mathbf{R}}(\alpha) = \begin{bmatrix} \hat{\mathbf{R}}_{yy}(\alpha) & \hat{\mathbf{R}}_{yx}(\alpha) \\ \hat{\mathbf{R}}_{yx}^H(\alpha) & \hat{\mathbf{R}}_{xx}(\alpha) \end{bmatrix}. \tag{13}$$

It is well known that the determinant of a block matrix like (13) can be expressed in terms of its Schur complement [28]

$$\left|\hat{\mathbf{R}}(\alpha)\right| = \left|\hat{\mathbf{R}}_{xx}(\alpha) - \hat{\mathbf{R}}_{yx}^H(\alpha)\hat{\mathbf{R}}_{yy}^{-1}(\alpha)\hat{\mathbf{R}}_{yx}(\alpha)\right|\left|\hat{\mathbf{R}}_{yy}(\alpha)\right|.$$

Using the above result, the cost function in (4) is equivalent to

$$\ln\left|\hat{\mathbf{R}}(\alpha)\right| - \ln\left|\hat{\mathbf{R}}_{yy}(\alpha)\right|. \tag{14}$$

By using (5)–(7), along with new definitions of regression vectors

$$\mathbf{s}_{P+1}(n) = \left[\mathbf{t}^T(n), \mathbf{s}^T(n)\right]^T \tag{15}$$

$$\mathbf{x}_{k,P+1}(n) = \left[\mathbf{y}_k^T(n), \mathbf{x}_k^T(n)\right]^T \tag{16}$$

$\hat{\mathbf{R}}(\alpha)$ can be decomposed into an α-dependent component and an α-independent one

$$\hat{\mathbf{R}}(\alpha) = (\mathbf{X}_0 - \alpha\mathbf{S})(\mathbf{X}_0 - \alpha\mathbf{S})^H + \sum_{k=1}^{K}\mathbf{X}_k\mathbf{X}_k^H \tag{17}$$

where the new steering matrix $\mathbf{S}$ and data matrix $\mathbf{X}_k$ are given as

$$\mathbf{S} = [\mathbf{s}_{P+1}(P),\ldots,\mathbf{s}_{P+1}(N-1)] \in \mathbb{C}^{J(P+1)\times(N-P)} \tag{18}$$

$$\mathbf{X}_k = [\mathbf{x}_{k,P+1}(P),\ldots,\mathbf{x}_{k,P+1}(N-1)], \quad k=0,1,\ldots,K. \tag{19}$$

Similarly, $\hat{\mathbf{R}}_{yy}(\alpha)$ can be decomposed as

$$\hat{\mathbf{R}}_{yy}(\alpha) = (\mathbf{Y}_0 - \alpha\mathbf{T})(\mathbf{Y}_0 - \alpha\mathbf{T})^H + \sum_{k=1}^{K}\mathbf{Y}_k\mathbf{Y}_k^H \tag{20}$$

where

$$\mathbf{T} = [\mathbf{t}(P),\ldots,\mathbf{t}(N-1)] \in \mathbb{C}^{JP\times(N-P)} \tag{21}$$

$$\mathbf{Y}_k = [\mathbf{y}_k(P),\ldots,\mathbf{y}_k(N-1)],\ k=0,1,\ldots,K. \tag{22}$$

Using (17) and (20), an asymptotically equivalent expression for (14) is derived in Appendix I

$$\ln\left[1+\mathrm{tr}\left\{(\mathbf{X}_0\mathbf{P}_S - \alpha\mathbf{S})^H\hat{\mathbf{R}}_X^{-1}(\mathbf{X}_0\mathbf{P}_S - \alpha\mathbf{S})\right\}\right] - \ln\left[1+\mathrm{tr}\left\{(\mathbf{Y}_0\mathbf{P}_T - \alpha\mathbf{T})^H\hat{\mathbf{R}}_Y^{-1}(\mathbf{Y}_0\mathbf{P}_T - \alpha\mathbf{T})\right\}\right] \tag{23}$$

where

$$\hat{\mathbf{R}}_X = \mathbf{X}_0\mathbf{P}_S^{\perp}\mathbf{X}_0^H + \sum_{k=1}^{K}\mathbf{X}_k\mathbf{X}_k^H \tag{24}$$

$$\hat{\mathbf{R}}_Y = \mathbf{Y}_0 \mathbf{P}_{\bar{T}}^{\perp} \mathbf{Y}_0^H + \sum_{k=1}^{K} \mathbf{Y}_k \mathbf{Y}_k^H \tag{25}$$

with $\mathbf{P}_{\bar{S}}^{\perp}$ denoting the projection matrix to the orthogonal complement of the range of $\mathbf{S}^H$

$$\mathbf{P}_{\bar{S}}^{\perp} = \mathbf{I} - \mathbf{P}_S = \mathbf{I} - \mathbf{S}^H (\mathbf{S}^H)^{\dagger} \tag{26}$$

where $(\mathbf{S}^H)^{\dagger}$ denotes the Moore–Penrose pseudoinverse of $\mathbf{S}^H$ while the other projection matrix $\mathbf{P}_{\bar{T}}^{\perp}$ is similarly defined using the matrix $\mathbf{T}$.

Based on the asymptotic expression (23), a closed-form estimate of the amplitude is given by (see Appendix II)

$$\hat{\alpha} = \frac{\mathrm{tr}\left\{\mathbf{S}^H \hat{\mathbf{R}}_X^{-1} \mathbf{X}_0 - \mathbf{T}^H \hat{\mathbf{R}}_Y^{-1} \mathbf{Y}_0\right\}}{\mathrm{tr}\left\{\mathbf{S}^H \hat{\mathbf{R}}_X^{-1} \mathbf{S} - \mathbf{T}^H \hat{\mathbf{R}}_Y^{-1} \mathbf{T}\right\}}. \tag{27}$$

Note that (27) is also an AML estimate, since the underlying approximations (see Appendixes I and II) of the likelihood function were made in the asymptotic sense. For convenience, the AML estimator of [7] is henceforth referred to as **AML1**, whereas the new amplitude estimate (27) is referred to as **AML2**. While both estimators are AML, it should be noted that, unlike AML1, which involves a two-step estimation process initialized by the LS estimator, AML2 is in closed form, requiring only a one-step calculation. As we show in Section V, the two estimators perform similarly when the data size is large; however, in the more challenging case with limited data, AML1 yields a notably worse performance due to the coarse initial estimate provided by the LS estimator.

IV. New Parametric GLRT

Given the AML2 amplitude estimate (27), the spatial covariance matrix estimates (9) and (10) can be obtained in closed form, which also lead to a closed-form expression of the parametric GLRT test statistic. In particular, we show in Appendix III that the test statistic (8) can be expressed as

$$\frac{\left|\sum_{n=P}^{N-1}\left[\mathbf{s}_{P+1}^H(n)\hat{\mathbf{R}}_X^{-1}\mathbf{x}_{0,P+1}(n) - \mathbf{t}^H(n)\hat{\mathbf{R}}_Y^{-1}\mathbf{y}_0(n)\right]\right|^2}{\sum_{n=P}^{N-1}\left[\mathbf{s}_{P+1}^H(n)\hat{\mathbf{R}}_X^{-1}\mathbf{s}_{P+1}(n) - \mathbf{t}^H(n)\hat{\mathbf{R}}_Y^{-1}\mathbf{t}(n)\right]} \triangleq \mathrm{GLR}. \tag{28}$$

To gain additional insight into the test statistic and the behavior of the general parametric GLRT, it is shown in Appendix IV that the test statistic can be equivalently expressed as

$$\mathrm{GLR} = \frac{\left|\sum_{n=P}^{N-1} \mathbf{s}_{P+1}^H(n)\mathbf{W}\mathbf{x}_{0,P+1}(n)\right|^2}{\sum_{n=P}^{N-1} \mathbf{s}_{P+1}^H(n)\mathbf{W}\mathbf{s}_{P+1}(n)} \tag{29}$$

where $\mathbf{s}_{P+1}(n)$ and $\mathbf{x}_{0,P+1}(n)$ are $J(P+1)\times 1$ vectors defined in (15) and (16) and $\mathbf{W}$ is a block whitening matrix

$$\mathbf{W} = \begin{bmatrix} \mathbf{W}_1 & \mathbf{W}_2 \\ \mathbf{W}_2^H & \mathbf{W}_3 \end{bmatrix} \tag{30}$$

with individual component matrix given by (52)–(54) in Appendix IV.

From (29), it is seen that the parametric GLRT performs a partial spatiotemporal whitening across $J(P+1)$ dimensions (i.e., the size of the regression vectors $\mathbf{x}_{0,P+1}$ formed from the test signal) using the whitening matrix $\mathbf{W}$. Recall that a fully adaptive STAP detector such as Kelly's GLRT [3] performs a joint spatiotemporal whitening across all JN dimensions, whereas the parametric Rao or PAMF detector performs successive (as opposed to joint) whitening, i.e., temporal whitening followed by spatial whitening [14], [15]. Hence, the parametric GLRT is positioned between the two cases. This allows the parametric GLRT to utilize a parametric model and provide data efficiency just like the Rao, meanwhile exploiting more degrees of freedom for more effective interference rejection and detection. This corroborates earlier numerical results [16], which shows that the parametric GLRT in general outperforms the parametric Rao when the data available for estimation become very limited.

V. Numerical Examples

In this section, several simulation results are provided to illustrate the performance of the proposed estimation and detection techniques. We consider simulated data generated using an AR model and the KASSPER data [29], which were obtained from more realistic clutter model. For the first case, the disturbance signal is generated as a multichannel AR(2) process with AR coefficient $\mathbf{A}$ and spatial covariance matrix $\mathbf{Q}$; these parameters are set to ensure that the AR process is stable and $\mathbf{Q}$ is a valid covariance matrix, but otherwise randomly selected. The signal vector $\mathbf{s}$ corresponds to a uniform equispaced linear array with randomly selected normalized spatial and Doppler frequencies. The signal-to-(interference plus noise) ratio (SINR) is defined as

$$\mathrm{SINR} = |\alpha|^2 \mathbf{s}^H \mathbf{R}^{-1} \mathbf{s}. \tag{31}$$

A. Estimation

We focus here on the challenging case with zero range training, i.e., $K = 0$, which is of great interest for applications in heterogeneous environments. Under this setup, we consider two subcases with 1) $N = 32$, i.e., a moderate value for the number of pulses within a CPI; and 2) $N = 16$, a more limited scenario. For both cases, we compare the **LS** estimator (12), **AML1** of [16], **AML2** (27), and the **ML** estimator (4) initialized by AML1 (this consideration is motivated by the fact that **AML1** provides the best known initial estimate prior to this work).

Fig. 1 presents the mean-squared error (MSE) of the amplitude estimate $\hat{\alpha}$ obtained by each estimator, along with the Cramér–Rao bound (CRB), a lower bound for any unbiased estimator, versus the SINR when $N = 32$ and $J = 4$. It is seen that, in this case, the AML1 and AML2 amplitude estimates are nearly identical to the ML estimate, while the LS amplitude estimate shows the worst performance among all estimators.

The results for the case of $N = 16$ are shown in Fig. 2. We see that the AML1 estimate is worse than the AML2 estimate in the current case, whereas the ML estimate is the worst due

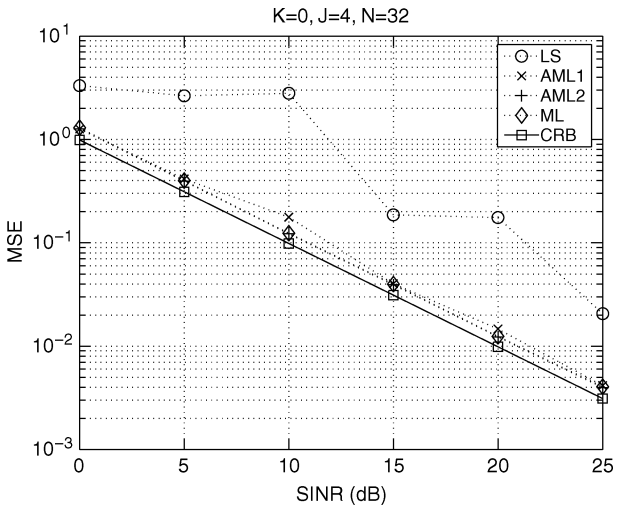

Fig. 1. MSEs of amplitude estimate $\hat{\alpha}$ versus SINR when $J = 4$, $N = 32$, and $K = 0$.

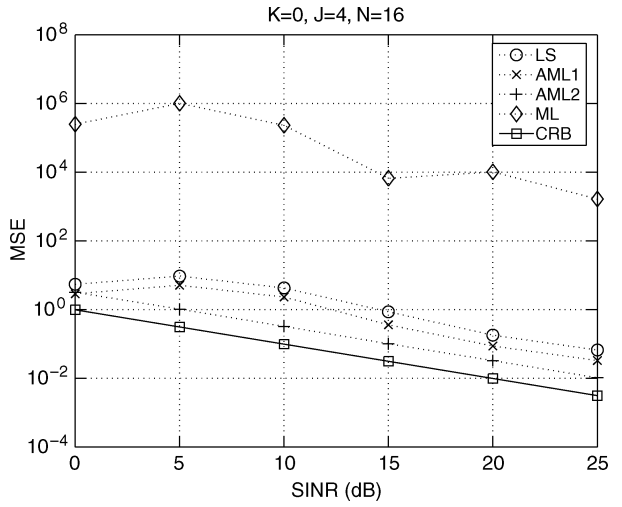

Fig. 2. MSEs of amplitude estimate $\hat{\alpha}$ versus SINR when $J = 4$, $N = 16$, and $K = 0$.

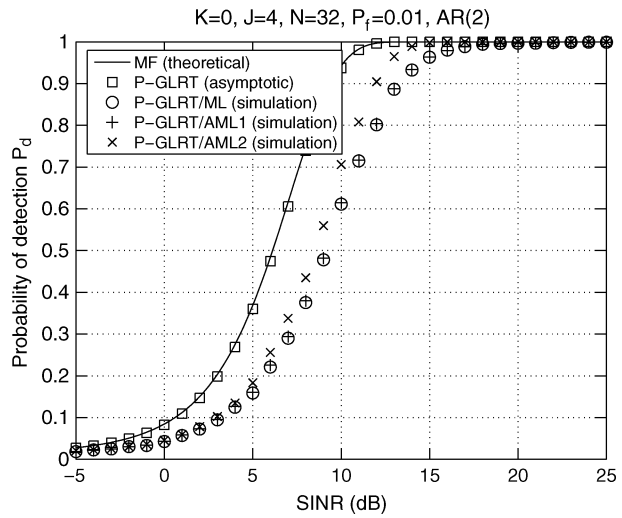

Fig. 3. Probability of detection $P_{\rm d}$ versus SINR when $P_{\rm f} = 0.01$, $J = 4$, $N = 32$, and $K = 0$.

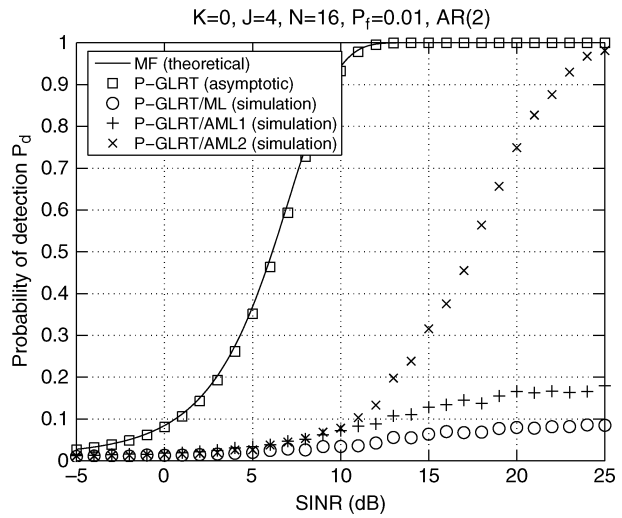

Fig. 4. Probability of detection $P_{\rm d}$ versus SINR when $P_{\rm f} = 0.01$, $J = 4$, $N = 16$, and $K = 0$.

to inaccurate initialization and local convergence. This clearly shows the limitation of the iterative search-based ML estimator.

B. Detection

Here, we report the detection performance under the same setup as in Figs. 1 and 2. We compare the various parametric GLRTs, including $\mathbf{GLRT/AML1}$ [i.e., GLRT (8) with the AML1 estimator], $\mathbf{GLRT/ML}$ [GLRT (8) with the ML estimator], and $\mathbf{GLRT/AML2}$ [GLRT (28) with the new AML2 estimator]. Also included in the comparison are the asymptotic result provided by the parametric GLRT (see [16]) and the ideal MF, which assumes exact knowledge of $\mathbf{R}$ and, therefore, cannot be used in practice but offers a baseline for comparison. Here, we set the probability of false alarm as $P_{\rm f} = 0.01$.

Fig. 3 shows the probability of detection $P_{\rm d}$ versus SINR for various detectors when the number of temporal samples $N = 32$ and no range training data is available. It is seen that the GLRT/AML2 slightly outperforms the GLRT/ML and GLRT/AML1, but overall they are quite similar, and all are within 3 dB from the ideal MF detector. The limited sample case of $N = 16$ is depicted in Fig. 4, where the GLRT/AML2 achieves significantly better results than the GLRT/ML and GLRT/AML1. The poor performance of the GLRT/ML is due to the poor amplitude estimate, which, as shown earlier in Fig. 2, is caused by inaccurate initialization and local convergence.

C. KASSPER Dataset

In the above simulation, the disturbance is generated by an AR process, which matches the assumed model of the parametric detectors. To show the detection performance in a more realistic environment, we use the KASSPER dataset, which, first, is not generated from an AR model and, in addition, contains many challenging real-world effects, including heterogeneous terrain, array errors, and dense ground targets (see [29] for a detailed description of the KASSPER dataset).

Fig. 5 shows the probability of detection versus SINR in the training-free $K = 0$ case, where the number of spatial channels is $J = 11$ and the number of temporal samples is $N = 32$. All

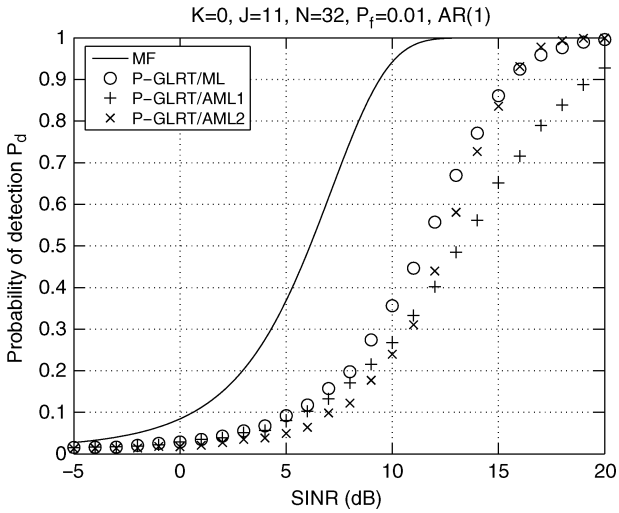

Fig. 5. Probability of detection $P_{\rm d}$ versus SINR for the KASSPER dataset when $P_{\rm f} = 0.01$, $J = 11$, $N = 32$, and $K = 0$.

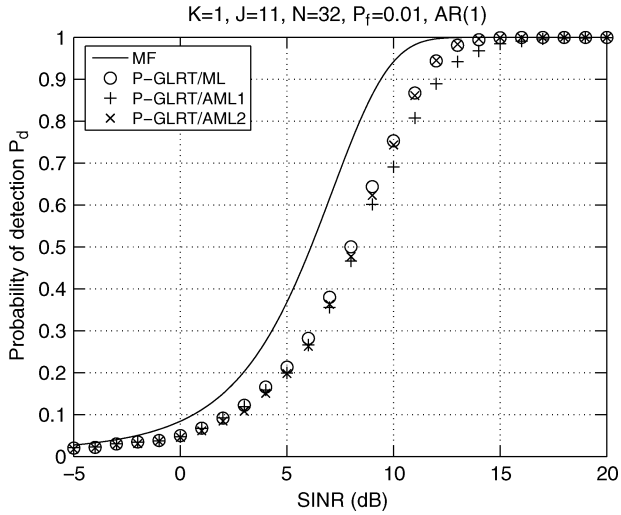

Fig. 6. Probability of detection $P_{\rm d}$ versus SINR for the KASSPER dataset when $P_{\rm f} = 0.01$, $J = 11$, $N = 32$, and $K = 1$.

parametric detectors use an AR(1) process to model and estimate the disturbance. Results show that the new GLRT/AML2 generally outperforms GLRT/AML1 and is slightly better than GLRT/ML at high SINR.

The parametric GLRT effectively trades range training for temporal pulses within a CPI and if the number N of the latter is large relative to the number of unknowns to be estimated, determined by J (number of spatial channels) and P (AR model order). In general, for low-order AR models, the parametric GLRT can provide good detection performance (e.g., within 3 dB from the MF bound) if $N/J > 5$ [16]. This is not the case for Fig. 5, where $N/J \approx 3$ and we see a performance gap of about 7 dB. To close the gap, we consider the case when the parametric detectors utilize $K = 1$ range training signal while the other parameters are kept the same.

There are two guard cells between the test cell and the training cell. In practical radar systems, K is usually an even number, as training data are often taken from both sides of the test cell. Here, we choose $K = 1$ corresponding to a more restrictive case.

The results are depicted in Fig. 6. It should be noted that in the KASSPER data, clutter across range cells is not i.i.d. [29]. Still, a small amount of training is useful to the parametric detector in the current case, all yielding improved detection performance less than 3 dB from the MF bound. This is due to the fact that the effect of clutter variation across a small area (i.e., for small K) is negligible. On the other hand, for a data-demanding nonparametric covariance matrix-based STAP detector, K has to be very large, in which case the effect of range-dependent clutter on such detectors can no longer be neglected [29].

VI. Conclusion

A new parametric GLRT for multichannel adaptive signal detection has been proposed. The detector builds on a new closed-form solution for the underlying nonlinear estimation problem. The new parametric GLRT obviates the need for initial parameter estimation as required by an earlier scheme, is computationally simpler, and provides generally improved detection performance when training data are limited. Due to its data efficiency, our new parametric GLRT and the underlying estimator are particularly useful for detection and estimation in training limited environments.

Appendix I
Derivation of (23)

Starting from (14), the determinant of $\hat{\mathbf{R}}(\alpha)$ can be written as

$$\begin{aligned}&\left|(\mathbf{X}_0-\alpha\mathbf{S})(\mathbf{X}_0-\alpha\mathbf{S})^H+\sum_{k=1}^{K}\mathbf{X}_k\mathbf{X}_k^H\right|\\&\quad=\Big|(\mathbf{X}_0\mathbf{P}_S-\alpha\mathbf{S})(\mathbf{X}_0\mathbf{P}_S-\alpha\mathbf{S})^H\\&\qquad+\mathbf{X}_0\mathbf{P}_S^{\perp}\mathbf{X}_0^H+\sum_{k=1}^{K}\mathbf{X}_k\mathbf{X}_k^H\Big|\\&\quad=\left|(\mathbf{X}_0\mathbf{P}_S-\alpha\mathbf{S})(\mathbf{X}_0\mathbf{P}_S-\alpha\mathbf{S})^H\hat{\mathbf{R}}_X^{-1}+\mathbf{I}\right|\cdot|\hat{\mathbf{R}}_X|.\end{aligned}\quad(32)$$

Consider the idempotent matrices $\mathbf{P}_S$ and $\mathbf{P}_S^{\perp}$ and assuming the number of sample data is large enough, i.e., $N \gg 1$, we have

$$\text{rank}(\mathbf{P}_S) \le J(P+1) \text{ and rank } \left(\mathbf{P}_S^{\perp}\right) \ge N-P \quad(33)$$

where rank$(\cdot)$ denotes the rank of a matrix. Then, we have [26]

$$(\mathbf{X}_0\mathbf{P}_S-\alpha\mathbf{S})(\mathbf{X}_0\mathbf{P}_S-\alpha\mathbf{S})^H\hat{\mathbf{R}}_X^{-1}=O\left(\frac{1}{N-P}\right)\ll 1.\quad(34)$$

Let $\{\lambda_m\}_{m=1}^{M}$ denote the eigenvalues of the matrix (34), which satisfies $0 \le \lambda_m \ll 1$ according to (34). Then

$$\begin{aligned}&\left|(\mathbf{X}_0\mathbf{P}_S-\alpha\mathbf{S})(\mathbf{X}_0\mathbf{P}_S-\alpha\mathbf{S})^H\hat{\mathbf{R}}_X^{-1}+\mathbf{I}\right|\\&\quad=\prod_{m=1}^{M}(1+\lambda_m)\\&\quad\overset{a}{\approx}1+\sum_{m=1}^{M}\lambda_m\\&\quad=1+\text{tr}\left[(\mathbf{X}_0\mathbf{P}_S-\alpha\mathbf{S})^H\hat{\mathbf{R}}_X^{-1}(\mathbf{X}_0\mathbf{P}_S-\alpha\mathbf{S})\right]\end{aligned}\quad(35)$$

where the approximation (a) holds in a first-order sense. Similarly, the determinant of $\hat{\mathbf{R}}_{yy}(\alpha)$ can be expressed as

$$\left|\hat{\mathbf{R}}_{yy}(\alpha)\right| = \left|(\mathbf{Y}_0\mathbf{P}_T - \alpha\mathbf{T})(\mathbf{Y}_0\mathbf{P}_T - \alpha\mathbf{T})^H\hat{\mathbf{R}}_Y^{-1} + \mathbf{I}\right| \cdot |\hat{\mathbf{R}}_Y| \tag{36}$$

and

$$\begin{aligned}&\left|(\mathbf{Y}_0\mathbf{P}_T - \alpha\mathbf{T})(\mathbf{Y}_0\mathbf{P}_T - \alpha\mathbf{T})^H\hat{\mathbf{R}}_Y^{-1} + \mathbf{I}\right| \\ &\quad\approx 1 + \operatorname{tr}\left\{(\mathbf{Y}_0\mathbf{P}_T - \alpha\mathbf{T})^H\hat{\mathbf{R}}_Y^{-1}(\mathbf{Y}_0\mathbf{P}_T - \alpha\mathbf{T})\right\}.\end{aligned} \tag{37}$$

Then, combining (32) and (35)–(37) and ignoring the items independent of α result in the asymptotically equivalent expression in (23).

Appendix II
Derivation of the Amplitude Estimator

Following Appendix I and noting that

$$\operatorname{tr}\left\{(\mathbf{X}_0\mathbf{P}_S - \alpha\mathbf{S})^H\hat{\mathbf{R}}_X^{-1}(\mathbf{X}_0\mathbf{P}_S - \alpha\mathbf{S})\right\} \ll 1 \tag{38}$$

and

$$\operatorname{tr}\left\{(\mathbf{Y}_0\mathbf{P}_T - \alpha\mathbf{T})^H\hat{\mathbf{R}}_Y^{-1}(\mathbf{Y}_0\mathbf{P}_T - \alpha\mathbf{T})\right\} \ll 1 \tag{39}$$

we can approximate (23) as

$$\begin{aligned}F_1(\alpha) =& \operatorname{tr}\left\{(\mathbf{X}_0\mathbf{P}_S - \alpha\mathbf{S})^H\hat{\mathbf{R}}_X^{-1}(\mathbf{X}_0\mathbf{P}_S - \alpha\mathbf{S})\right\} \\ &- \operatorname{tr}\left\{(\mathbf{Y}_0\mathbf{P}_T - \alpha\mathbf{T})^H\hat{\mathbf{R}}_Y^{-1}(\mathbf{Y}_0\mathbf{P}_Y - \alpha\mathbf{T})\right\}\end{aligned} \tag{40}$$

where the approximation $\ln(1+x) \approx x$, for $x \ll 1$, was invoked. The cost function $F_1(\alpha)$ is a quadratic function with respect to α. It is easy to show that minimizing (40) with respect to α leads to the AML2 amplitude estimate $\hat{\alpha}$ given by (27).

Appendix III
Derivation of the New Parametric GLRT

Using the Schur complements, we can write (8) as

$$\begin{aligned}&\ln\frac{|\hat{\mathbf{Q}}_{\mathrm{ML},0}|}{|\hat{\mathbf{Q}}_{\mathrm{ML},1}|} \\ &\quad= \ln\frac{\left|\mathbf{X}_0\mathbf{X}_0^H + \sum_{k=1}^{K}\mathbf{X}_k\mathbf{X}_k^H\right|}{\left|\mathbf{Y}_0\mathbf{Y}_0^H + \sum_{k=1}^{K}\mathbf{Y}_k\mathbf{Y}_k^H\right|} \\ &\qquad- \ln\frac{\left|(\mathbf{X}_0 - \hat{\alpha}_{\mathrm{ML}}\mathbf{S})(\mathbf{X}_0 - \hat{\alpha}_{\mathrm{ML}}\mathbf{S})^H + \sum_{k=1}^{K}\mathbf{X}_k\mathbf{X}_k^H\right|}{\left|(\mathbf{Y}_0 - \hat{\alpha}_{\mathrm{ML}}\mathbf{T})(\mathbf{Y}_0 - \hat{\alpha}_{\mathrm{ML}}\mathbf{T})^H + \sum_{k=1}^{K}\mathbf{Y}_k\mathbf{Y}_k^H\right|} \\ &\quad\propto \ln\frac{\left|\mathbf{X}_0\mathbf{P}_S\mathbf{X}_0^H\hat{\mathbf{R}}_X^{-1} + \mathbf{I}\right|}{\left|\mathbf{Y}_0\mathbf{P}_t\mathbf{Y}_0^H\hat{\mathbf{R}}_Y^{-1} + \mathbf{I}\right|} \\ &\qquad- \ln\frac{\left|(\mathbf{X}_0\mathbf{P}_S - \hat{\alpha}_{\mathrm{ML}}\mathbf{S})(\mathbf{X}_0\mathbf{P}_S - \hat{\alpha}_{\mathrm{ML}}\mathbf{S})^H\hat{\mathbf{R}}_X^{-1} + \mathbf{I}\right|}{\left|(\mathbf{Y}_0\mathbf{P}_T - \hat{\alpha}_{\mathrm{ML}}\mathbf{T})(\mathbf{Y}_0\mathbf{P}_T - \hat{\alpha}_{\mathrm{ML}}\mathbf{T})^H\hat{\mathbf{R}}_Y^{-1} + \mathbf{I}\right|}.\end{aligned}$$

The right-hand side of the above equation can be further simplified using asymptotic approximations [see (35) and (36)]

$$\begin{aligned}&\ln\frac{|\hat{\mathbf{Q}}_{\mathrm{ML},0}|}{|\hat{\mathbf{Q}}_{\mathrm{ML},1}|} \\ &\quad\propto \operatorname{tr}\left\{\mathbf{P}_S^H\mathbf{X}_0^H\hat{\mathbf{R}}_X^{-1}\mathbf{X}_0\mathbf{P}_S\right\} - \operatorname{tr}\left\{\mathbf{P}_T^H\mathbf{Y}_0^H\hat{\mathbf{R}}_Y^{-1}\mathbf{Y}_0\mathbf{P}_T\right\} \\ &\qquad- \operatorname{tr}\left\{(\mathbf{X}_0\mathbf{P}_S - \hat{\alpha}_{\mathrm{ML}}\mathbf{S})^H\hat{\mathbf{R}}_X^{-1}(\mathbf{X}_0\mathbf{P}_S - \hat{\alpha}_{\mathrm{ML}}\mathbf{S})\right\} \\ &\qquad+ \operatorname{tr}\left\{(\mathbf{Y}_0\mathbf{P}_T - \hat{\alpha}_{\mathrm{ML}}\mathbf{T})^H\hat{\mathbf{R}}_Y^{-1}(\mathbf{Y}_0\mathbf{P}_T - \hat{\alpha}_{\mathrm{ML}}\mathbf{T})\right\}.\end{aligned}$$

Replacing the exact ML estimate with the AML2 amplitude estimation results in the approximate parametric GLRT

$$\mathrm{GLR} \approx \frac{\left|\operatorname{tr}\left(\mathbf{S}^H\hat{\mathbf{R}}_X^{-1}\mathbf{X}_0\right) - \operatorname{tr}\left(\mathbf{T}^H\hat{\mathbf{R}}_Y^{-1}\mathbf{Y}_0\right)\right|^2}{\operatorname{tr}\left(\mathbf{S}^H\hat{\mathbf{R}}_X^{-1}\mathbf{S}\right) - \operatorname{tr}\left(\mathbf{T}^H\hat{\mathbf{R}}_Y^{-1}\mathbf{T}\right)} \tag{41}$$

which is the matrix form of (28).

Appendix IV
Alternative Form of the Parametric GLRT

Let

$$\mathbf{S}_1 = [\mathbf{s}(P), \mathbf{s}(P+1), \ldots, \mathbf{s}(N-1)] \in \mathbb{C}^{J\times(N-P)} \tag{42}$$

and $\mathbf{X}_{k,1} \in \mathbb{C}^{J\times(N-P)}$ be similarly defined. The matrix $\mathbf{S}$ can be rewritten as $\mathbf{S}^H = [\mathbf{T}^H, \mathbf{S}_1^H]$, where $\mathbf{T} \in \mathbb{C}^{JP\times(N-P)}$ is given by (21). By invoking the formula of the block matrix pseudoinverse [30], we have

$$\mathbf{P}_S^{\perp} = \mathbf{I} - \left[\mathbf{T}^H\mathbf{S}_1^H\right]\begin{bmatrix}(\mathbf{T}^H)^{\dagger} - (\mathbf{T}^H)^{\dagger}\mathbf{S}_1^H(\mathbf{C}^{\dagger} + \mathbf{D}) \\ (\mathbf{C}^{\dagger} + \mathbf{D})\end{bmatrix} \tag{43}$$

where

$$\mathbf{C} = \left(\mathbf{I}_{N-P} - \mathbf{T}^H(\mathbf{T}^H)^{\dagger}\right)\mathbf{S}_1^H \in \mathbb{C}^{(N-P)\times J} \tag{44}$$

and

$$\begin{aligned}\mathbf{D} = (\mathbf{I}_J - \mathbf{C}^{\dagger}\mathbf{C})\left[\mathbf{I}_J + (\mathbf{I}_J - \mathbf{C}^{\dagger}\mathbf{C})\mathbf{S}_1\mathbf{T}^{\dagger}\mathbf{S}_1^H(\mathbf{I}_J - \mathbf{C}^{\dagger}\mathbf{C})\right]^{-1} \\ \times\mathbf{S}_1\mathbf{T}^{\dagger}\left(\mathbf{I}_{N-P} - \mathbf{S}_1^H\mathbf{C}^{\dagger}\right) \in \mathbb{C}^{J\times(N-P)}.\end{aligned} \tag{45}$$

Expanding (43) yields

$$\mathbf{P}_S^{\perp} = \mathbf{P}_T^{\perp}\left(\mathbf{I} - \mathbf{S}_1^H(\mathbf{C}^{\dagger} + \mathbf{D})\right) \triangleq \mathbf{P}_T^{\perp}(\mathbf{I} - \mathbf{E}). \tag{46}$$

From (24) and (25), the $\hat{\mathbf{R}}_X$ can be

$$\hat{\mathbf{R}}_X = \begin{bmatrix}\hat{\mathbf{R}}_{X,1} & \hat{\mathbf{R}}_{X,2} \\ \hat{\mathbf{R}}_{X,1}^H & \hat{\mathbf{R}}_{X,3}\end{bmatrix} \tag{47}$$

where

$$\hat{\mathbf{R}}_{X,1} = \hat{\mathbf{R}}_Y - \mathbf{Y}_0\mathbf{P}_T^{\perp}\mathbf{E}\mathbf{Y}_0^H \tag{48}$$

$$\hat{\mathbf{R}}_{X,2} = \mathbf{Y}_0\mathbf{P}_T^{\perp}(\mathbf{I} - \mathbf{E})\mathbf{X}_{0,1}^H + \sum_{k=1}^{K}\mathbf{Y}_k\mathbf{X}_{k,1}^H \tag{49}$$

$$\hat{\mathbf{R}}_{X,3} = \mathbf{X}_{0,1}\mathbf{P}_T^{\perp}(\mathbf{I} - \mathbf{E})\mathbf{X}_{0,1}^H + \sum_{k=1}^{K}\mathbf{X}_{k,1}\mathbf{X}_{k,1}^H. \tag{50}$$

Applying the block matrix inversion lemma twice, first on $\hat{\mathbf{R}}_X$ and then on $\hat{\mathbf{R}}_{X,1}$, we have

$$\hat{\mathbf{R}}_X^{-1} = \begin{bmatrix} \hat{\mathbf{R}}_Y^{-1} + \mathbf{W}_1 & \mathbf{W}_2 \\ \mathbf{W}_2^H & \mathbf{W}_3 \end{bmatrix} \tag{51}$$

where

$$\begin{aligned} \mathbf{W}_1 =& \hat{\mathbf{R}}_{X,1}^{-1}\hat{\mathbf{R}}_{X,2}\mathbf{W}_3\hat{\mathbf{R}}_{X,2}^H\hat{\mathbf{R}}_{X,1}^{-1} \\ & - \hat{\mathbf{R}}_Y^{-1}\mathbf{Y}_0\left(\mathbf{I} + \mathbf{P}_T^{\perp}\mathbf{E}\mathbf{Y}_0^H\hat{\mathbf{R}}_Y^{-1}\mathbf{Y}_0\right)^{-1} \\ & \times \mathbf{P}_T^{\perp}\mathbf{E}\mathbf{Y}_0^H\hat{\mathbf{R}}_Y^{-1} \end{aligned} \tag{52}$$

$$\mathbf{W}_2 = -\hat{\mathbf{R}}_{X,1}^{-1}\hat{\mathbf{R}}_{X,2}\mathbf{W}_3 \tag{53}$$

$$\mathbf{W}_3 = \left(\hat{\mathbf{R}}_{X,3} - \hat{\mathbf{R}}_{X,2}^H\hat{\mathbf{R}}_{X,1}^{-1}\hat{\mathbf{R}}_{X,2}\right)^{-1}. \tag{54}$$

Inserting the above results in (28) followed by simple manipulations, we can see that the parametric GLRT test statistic (28) is equivalent to (29).

ACKNOWLEDGMENT

The authors would like to thank Dr. M. Rangaswamy of the AFRL for his helpful comments and suggestions on this work.

REFERENCES

[1] J. Ward, Space-time adaptive processing for airborne radar MIT Lincoln Lab., Tech. Rep. 1015, Dec. 1994.
[2] I. S. Reed, J. D. Mallett, and L. E. Brennan, "Rapid convergence rate in adaptive arrays," *IEEE Trans. Aerosp. Electron. Syst.*, vol. AES-10, no. 6, pp. 853–863, 1974.
[3] E. J. Kelly, "An adaptive detection algorithm," *IEEE Trans. Aerosp. Electron. Syst.*, vol. AES-22, pp. 115–127, Mar. 1986.
[4] F. C. Robey, D. R. Fuhrmann, E. J. Kelly, and R. Nitzberg, "A CFAR adaptive matched filter detector," *IEEE Trans. Aerosp. Electron. Syst.*, vol. 28, pp. 208–216, Jan. 1992.
[5] S. Kraut and L. L. Scharf, "The CFAR adaptive subspace detector is a scale-invariant GLRT," *IEEE Trans. Signal Process.*, vol. 47, pp. 2538–2541, Sep. 1999.
[6] S. Kraut, L. L. Scharf, and L. T. McWhorter, "Adaptive subspace detectors," *IEEE Trans. Signal Process.*, vol. 49, pp. 1–16, Jan. 2001.
[7] L. Cai and H. Wang, "On adaptive filtering with the CFAR feature and its performance sensitivity to non-Gaussian interference," in *Proc. 24th Annu. Conf. Inf. Sci. Syst.*, Princeton, NJ, Mar. 1990, pp. 558–563.
[8] W. Chen and I. S. Reed, "A new CFAR detection test for radar," *Digital Signal Process.*, vol. 1, no. 4, pp. 198–214, 1991.
[9] J. S. Goldstein and I. S. Reed, "Reduced-rank adaptive filtering," *IEEE Trans. Signal Process.*, vol. 45, pp. 492–496, Feb. 1997.
[10] J. S. Goldstein, I. S. Reed, and P. A. Zulch, "Multistage partially adaptive STAP CFAR detection algorithm," *IEEE Trans. Aerosp. Electron. Syst.*, vol. 35, pp. 645–661, Apr. 1999.
[11] J. Guerci, J. S. Goldstein, and I. S. Reed, "Optimal and adaptive reduced-rank STAP," *IEEE Trans. Aerosp. Electron. Syst.*, vol. 36, pp. 647–663, Apr. 2000.
[12] M. Rangaswamy and J. H. Michels, "A parametric multichannel detection algorithm for correlated non-Gaussian random processes," in *Proc. 1997 IEEE Nat. Radar Conf.*, Syracuse, NY, May 1997, pp. 349–354.
[13] A. L. Swindlehurst and P. Stoica, "Maximum likelihood methods in radar array signal processing," *Proc. IEEE*, vol. 86, pp. 421–441, Feb. 1998.
[14] J. R. Román, M. Rangaswamy, D. W. Davis, Q. Zhang, B. Himed, and J. H. Michels, "Parametric adaptive matched filter for airborne radar applications," *IEEE Trans. Aerosp. Electron. Syst.*, vol. 36, no. 2, pp. 677–692, Apr. 2000.
[15] K. J. Sohn, H. Li, and B. Himed, "Parametric Rao test for multichannel adaptive signal detection," *IEEE Trans. Aerosp. Electron. Syst.*, vol. 43, pp. 920–933, Jul. 2007.
[16] K. J. Sohn, H. Li, and B. Himed, "Parametric GLRT for multichannel adaptive signal detection," *IEEE Trans. Signal Process.*, vol. 55, pp. 5351–5360, Nov. 2007.
[17] K. J. Sohn, H. Li, and B. Himed, "Recursive parametric tests for multichannel adaptive signal detection," *IET Radar, Sonar Navig.*, vol. 2, no. 1, pp. 63–70, Feb. 2008.
[18] S. L. Marple, Jr., P. M. Corbell, and M. Rangaswamy, "Multi-channel parametric estimator fast block matrix inverses," in *Proc. IEEE Int. Conf. Acoust., Speech Signal Process.*, Honolulu, HI, Apr. 2007.
[19] S. L. Marple, Jr., P. M. Corbell, and M. Rangaswamy, "Multi-channel fast parametric algorithms and performance for adaptive radar," in *Proc. 41th Asilomar Conf. Signals, Syst., Comput.*, Pacific Grove, CA, Nov. 2007.
[20] S. L. Marple, Jr., P. M. Corbell, and M. Rangaswamy, "Performance tradeoffs for multi-channel parametric adaptive radar algorithms," in *Proc. 2008 Int. Conf. Radar*, Rome, Italy, Sep. 2008.
[21] Y. I. Abramovich, N. K. Spencer, and M. Turley, "Order estimation and discrimination between stationary and time-varying (TVAR) autoregressive models," *IEEE Trans. Signal Process.*, vol. 55, pp. 2861–2876, Jun. 2007.
[22] Y. I. Abramovich, N. K. Spencer, and M. Turley, "Time-varying autoregressive (TVAR) models for multiple radar observations," *IEEE Trans. Signal Process.*, vol. 55, no. 4, pp. 1298–1311, Apr. 2007.
[23] K. J. Sohn, H. Li, B. Himed, and J. S. Markow, "Performance of multichannel parametric detectors with MCARM data," in *Proc. 2007 IET Int. Conf. Radar Syst.*, Edinburgh, U.K., Oct. 2007.
[24] P. Wang, K. J. Sohn, H. Li, and B. Himed, "Performance evaluation of parametric Rao and GLRT detectors with KASSPER and bistatic data," in *Proc. 2008 IEEE Radar Conf.*, Rome, Italy, May 2008.
[25] J. Li, G. Liu, N. Jiang, and P. Stoica, "Moving target feature extraction for airborne high-range resolution phased-array radar," *IEEE Trans. Signal Process.*, vol. 49, pp. 277–289, Feb. 2001.
[26] Y. Jiang, P. Stoica, and J. Li, "Array signal processing in the known waveform and steering vector case," *IEEE Trans. Signal Process.*, vol. 52, pp. 23–35, Jan. 2004.
[27] S. M. Kay, *Modern Spectral Estimation: Theory and Application*. Englewood Cliffs, NJ: Prentice-Hall, 1988.
[28] R. A. Horn and C. R. Johnson, *Matrix Analysis*. Cambridge, U.K.: Cambridge Univ. Press, 1985.
[29] J. S. Bergin and P. M. Techau, High-fidelity site-specific radar simulation: KASSPER'02 Workshop Datacube Information Systems Laboratories, Inc., Vienna, VA, Tech. Rep. ISL-SCRD-TR-02-105, May 2002.
[30] G. H. Golub and C. F. Van Loan, *Matrix Computations*, 3rd ed. Baltimore, MD: Johns Hopkins Univ. Press, 1996.

Pu Wang (S'05) received the B.Eng. and M.Eng. degrees in electrical engineering from the University of Electronic Science and Technology of China (UESTC), Chengdu, China, in 2003 and 2006, respectively. He is currently pursuing the Ph.D. degree at the Department of Electrical and Computer Engineering, Stevens Institute of Technology, Hoboken, NJ.

He was a Research Assistant from January 2007 to December 2007 and a Teaching Assistant from January 2008 to December 2008 at the Department of Electrical and Computer Engineering, Stevens Institute of Technology. His current research interests include statistical signal processing and its applications, with focus on detection and estimation, multichannel signal processing, and nonstationary signal processing.

Mr. Wang received the Francis T. Boesch Award in 2008 and the Outstanding Research Assistant Award in 2007 from Stevens Institute of Technology, the Excellent Master Thesis Award of Sichuan Province in 2007 from Sichuan Ministry of Education, and the Excellent Master Thesis Award of UESTC in 2006 from UESTC.

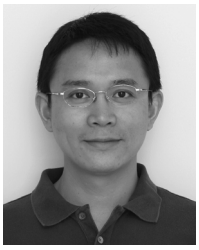

Hongbin Li (M'99–SM'08) received the B.S. and M.S. degrees from the University of Electronic Science and Technology of China, Chengdu, in 1991 and 1994, respectively, and the Ph.D. degree from the University of Florida, Gainesville, in 1999, all in electrical engineering.

From July 1996 to May 1999, he was a Research Assistant in the Department of Electrical and Computer Engineering, University of Florida. He was a Summer Visiting Faculty Member at the Air Force Research Laboratory in the summers of 2003, 2004, and 2009. Since 1999, he has been with the Department of Electrical and Computer Engineering, Stevens Institute of Technology, Hoboken, NJ, where he is an Associate Professor. His current research interests include statistical signal processing, wireless communications, and radars. He was a Guest Editor of the *EURASIP Journal on Applied Signal Processing*.

Dr. Li is a member of Tau Beta Pi and Phi Kappa Phi. He received the Harvey N. Davis Teaching Award in 2003 and the Jess H. Davis Memorial Award for excellence in research in 2001 from Stevens Institute of Technology, and the Sigma Xi Graduate Research Award from the University of Florida in 1999. He is a member of the Sensor Array and Multichannel Technical Committee of the IEEE Signal Processing Society. He is/has been an Editor or Associate Editor of the IEEE TRANSACTIONS ON WIRELESS COMMUNICATIONS, IEEE SIGNAL PROCESSING LETTERS, and IEEE TRANSACTIONS ON SIGNAL PROCESSING.

Braham Himed (S'88–M'90–SM'01–F'07) was born in Algiers, Algeria. He received the B.S. degree from Ecole Nationale Polytechnique of Algiers in 1984 and the M.S. and Ph.D. degrees from Syracuse University, Syracuse, NY, in 1987 and 1990, respectively, all in electrical engineering.

He is currently a Principal Electronics Engineer with the Sensors Directorate, Radar Signal Processing Branch, Air Force Research Laboratory, Dayton, OH. His research interests include detection, estimation, multichannel adaptive signal processing, time-series analyses, array processing, space-time adaptive processing, hot clutter mitigation, airborne and spaceborne radar, over the horizon radar, and below ground sensing.

Dr. Himed received the 2001 IEEE region award for his work on bistatic radar systems, algorithm development, and phenomenology. He is a member of the Aerospace and Electronic Systems Radar Systems Panel.